Numerical Modelling of Mixing Flow near an Ocean Outfall

S. Z. Ye* and J. Y. Tu
Australian Nuclear Science & Technology Organisation (ANSTO)
Private Mail Bag 1 Menai, NSW 2234, Australia

Abstract In this paper, a computational study of complex near-field mixing flow is described using two computational models representing a physical model performed previously in the laboratory and a prototype of Malabar outfall in Sydney, respectively. The theoretical hydraulic model used in this study is validated against experimental data and a fair agreement between the prediction and measurement is achieved. The comparisons between the numerical results obtained from the two computational models are made. It is found that for the mean behaviour of mixing flow near the outfall the agreement between the two results is reasonably satisfactory. However, the results at the turbulence level and its dissipation rate in both the spatial distribution pattern and magnitudes show the quite difference. This observation suggests that the physical modelling in the laboratory may produce significant errors in the prediction of contaminant transport and water quality where the prototype solute mixing may be strongly influenced by the turbulence kinetic energy and its dissipation rate.

1. INTRODUCTION

When wastes are released into the environment through ocean outfalls, it may be diluted rapidly, resulting in reductions of contaminant concentrations to safe levels within a short distance of the discharge -- an area called the "mixing zone." The initial dilution within the mixing zone is one of the most important characteristics in outfall design and environmental-impact assessment of effluent discharges (Proni et al., 1994). This can be achieved by discharging the effluent as a single turbulent jet diffuser or series of jet diffusers from the oceanbed.

Computational modelling is now playing the major role in providing an understanding of the physical process of waste transport within the mixing zone, the behaviour of the deepwater plumes, and the dilution of the released contaminant by water turbulence, to assist in the interpretation of the impact monitoring.

Throughout the past two decades there has been an increasing emphasis on using numerical models for flow and water quality studies, rather than physical models (scaled reproductions). This increasing emphasis on numerical rather than physical hydraulic models has occurred for a number of reasons, such as, physical models to be more expensive than numerical models; and not to be readily transportable, as compared to numerical models which can be distributed via floppy diskettes or internet. Also, physical models are not adaptable, in that a model of a particular estuary is unique to that estuary and cannot be used for any other estuary. In contrast, a validated and robust numerical model can be used for a wide range of estuarine studies and conditions, provided that the model limitations are appreciated and realistic.

Another important reason of emphasising on numerical rather than physical hydraulic models is that physical models have the overriding disadvantage of scaling. This constraint can be particularly critical for predicting contaminant transport and for water quality studies where, for example, the prototype solute mixing may be strongly influenced by the **turbulence level** and the **dissipation rate** - both of which may be significantly in error in the physical model.

This paper presents a computational study of near-field mixing flow using two computational models representing a physical model performed previously in the laboratory (Couriel and Wilkinson, 1993) and a prototype of Malabar outfall in Sydney, respectively. Before the detailed numerical experiments are carried out, the theoretical hydraulic model used in this study is validated against the experimental measurements given by Wu and Rajaratnam (1995). The aim of the present numerical experiments is to quantify the complex near field hydrodynamic behaviour, with detailed information of turbulence and its decay rate, of the ocean outfalls including the effects of discharge velocities and ambient currents. Of particular interest is to compare the results calculated from the two computational models. It is found that the agreement between the two results for the mean behaviour of mixing flow near the outfall is reasonably satisfactory. However, the significant difference between two results at the turbulence level and its dissipation rate is observed.

The next section provides the description of mathematical model including governing hydrodynamic equations, RNG (renormalisation group theory) based k-ε turbulence model, computational models for numerical experiments and boundary conditions, and numerical procedures. We shall then present detailed simulation results of numerical experiments for two computational models representing the laboratory physical model and the prototype. Concluding remarks are provided in the last section.

* Permanent address: Department of Fluid Mechanics and Hydraulics, North China Institute of Water Conservancy & Hydroelectric Power, Beijing, China

2. MATHEMATICAL MODEL

2.1 Governing Hydrodynamic Equations

The governing equations used to describe mixing flows near ocean outfalls in the Cartesian form are obtained by applying the Reynolds decomposition and time averaging the instantaneous continuity and momentum equations:

$$\frac{\partial}{\partial x_i}(u^i) = 0 \tag{1}$$

$$\frac{\partial}{\partial x_i}(\rho\, u^i u^j) = -\frac{\partial P}{\partial x_i} + \frac{\partial}{\partial x_i}(\rho\, \nu_l \frac{\partial}{\partial x_i} u^j) - \frac{\partial}{\partial x_i}(\rho\, \overline{u'^i u'^j}) \tag{2}$$

where ρ ,u ,u' and P are fluid density, mean velocity, fluctuating velocity and dynamic pressure, respectively. ν_l is fluid laminar viscosity.

2.2 Turbulence Model

In the above governing equations, there are more unknowns than equations due to the loss of information inherent in the averaging process. When the eddy-viscosity model is used, the Reynolds stresses are

$$\overline{u'^i u'^j} = -\nu_t(\frac{\partial u^i}{\partial x_j} + \frac{\partial u^j}{\partial x_i}) + \frac{2}{3} k \delta_{ij} \tag{3}$$

where ν_t is turbulent or 'eddy' viscosity of fluid which is evaluated by $(\nu_{eff} - \nu_l)$, where the effective viscosity ν_{eff} is computed by

$$\nu_{eff} = \nu_l (1 + \sqrt{\frac{C_\mu}{\nu_l}} \frac{k}{\sqrt{\varepsilon}})^2 \tag{4}$$

The kinetic energy of the turbulence, k, and its dissipation rate, ε, are governed by separate transport equations. A recently developed turbulence model, the dynamic renormalization group theory (RNG) based k-ε turbulence model (Orszag et al.,1993) is employed. The RNG-based k-ε turbulence model contains very few empirically adjustable parameters and is therefore applicable to a wide range of flow situations. The RNG theory models the k and ε transport equations as:

$$\frac{\partial}{\partial x_i}(\rho\, u^i k) = \frac{\partial}{\partial x_i}(\alpha\rho\, \nu_t \frac{\partial k}{\partial x_i}) + P_k - \rho\, \varepsilon \tag{5}$$

$$\frac{\partial}{\partial x_i}(\rho\, u^i \varepsilon) = \frac{\partial}{\partial x_i}(\alpha\rho\, \nu_t \frac{\partial \varepsilon}{\partial x_i}) + \frac{\varepsilon}{k}(C_{\varepsilon 1} P_k - C_{\varepsilon 2}\rho\, \varepsilon) - \rho\, R \tag{6}$$

where α is an inverse Prandtl number equal to 1.3929. The turbulence production P_k is evaluated by

$$P_k = \rho\, \nu_t (\frac{\partial u^i}{\partial x_j} + \frac{\partial u^j}{\partial x_i})\frac{\partial u^i}{\partial x_j} \tag{7}$$

The rate of strain term R in the ε-equation is expressed as

$$R = \frac{C_\mu \eta^3 (1 - \eta/\eta_0)}{1 + \beta\eta^3} \frac{\varepsilon^2}{k} \quad \text{and}$$

$$\eta = \frac{k}{\varepsilon}(2S_{ij}^2)^{1/2}, \qquad S_{ij} = \frac{1}{2}\left(\frac{\partial u^i}{\partial x_j} + \frac{\partial u^j}{\partial x_i}\right) \tag{8}$$

where $\beta = 0.015$, $\eta_0 = 4.38$. According to RNG theory, the constants in the turbulent transport equations are $C_\mu = 0.0845$, $C_{\varepsilon 1} = 1.42$ and $C_{\varepsilon 2} = 1.68$, respectively.

2.3 Computational Models and Boundary Conditions

Two computational models (laboratory scale and prototype) and corresponding numerical grids are created to investigate complex hydrodynamics behaviour near the outfall. Figure 1 shows the flow domain and the main recirculation zone behind the discharge port. The size of this recirculation zone will be characterised by its length L and lateral extent h. The water depth H is 0.75 m in the physical model and 22 m in the prototype, respectively. The local grids used in this study are shown in Figure 2, with a 120 x 60 nonuniformly distributed grid for the physical model and a 140 x 80 grid for the prototype model. Stretched grids are used to obtain an acceptable distribution of points near the diffusers and some solid cells (dead cells) are used for representing the outfall ports.

The boundary conditions are: Dirichlet boundary conditions are imposed at the inlet boundary; streamwise gradients (Neumann boundary conditions) for the variables are set to zero at the outlet plane; on the upper plane normal gradients are set to zero, and on the bottom plane no-slip boundary conditions for the velocities and the wall-function method (Roid, 1980) for determining the near wall values of k, ε are employed.

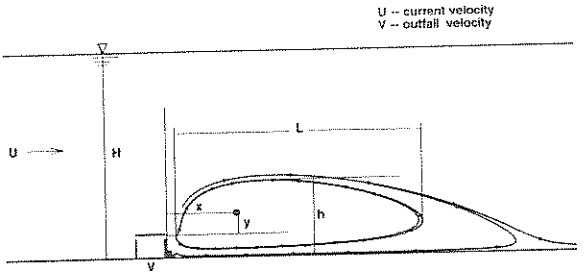

Figure 1 Illustration of flow configurations

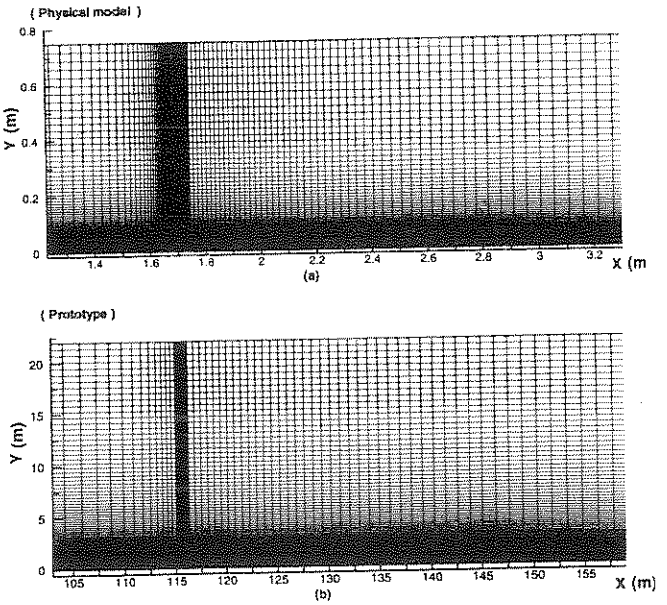

Figure 2 Computational grids in near ocean outfalls (a) for the physical model; (b) for the prototype

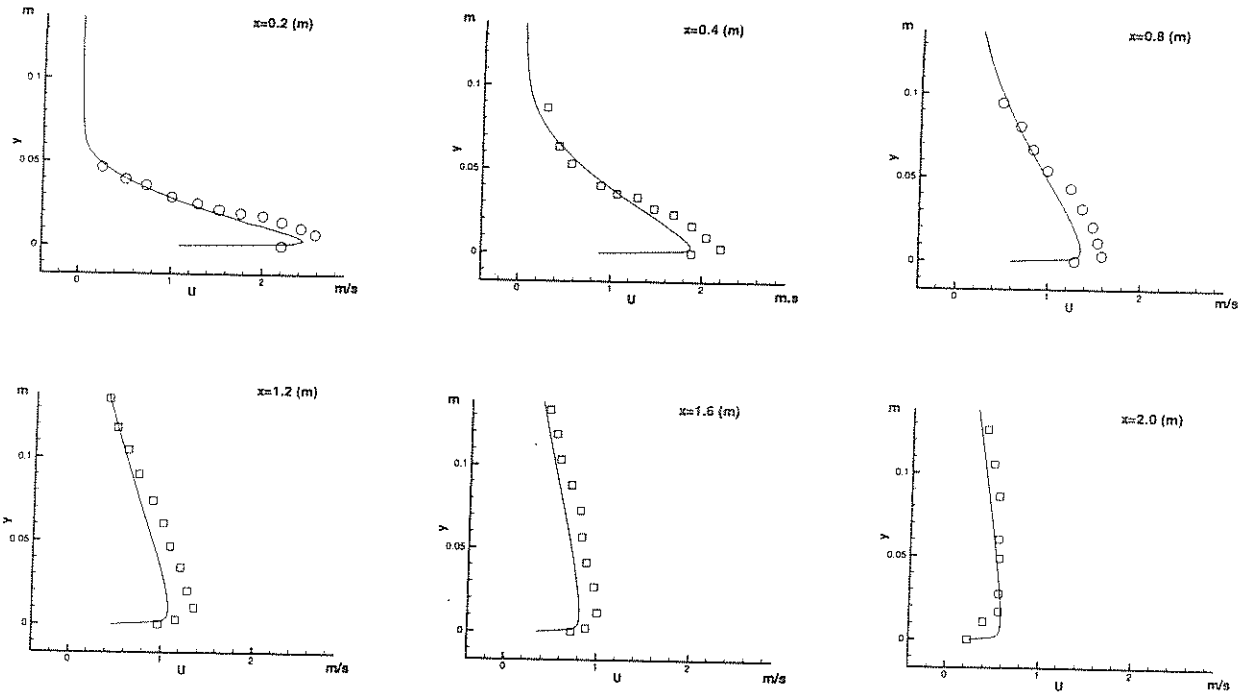

Figure 3 Comparison of predicted and measured velocity profiles

2.4 Numerical procedure

The governing equations are discretised using a finite volume formulation in generalised coordinate space with the metric information expressed in terms of area vectors (Tu and Fuchs, 1995). A semi-staggered grid system in which all velocity components are defined at the cell vertex while other scalar quantities, such as, pressure, turbulent kinetic energy and its dissipation rate are defined at the cell centre. A velocity potential correction is introduced to satisfy continuity equation and upgrade the pressure using a modified SIMPLE algorithm (Van Doormaal and Raithby, 1984). To approximate the convective terms at faces of the control volumes, a generalised QUICK convective differencing method (Fletcher, 1991) is used. The stored values at the centroids are interpolated and modified to calculate the flow flux at faces of the control volumes using the moment interpolation method (Rhie and Chow, 1983). The governing equations are solved sequentially by using a Multi-Grid procedure to obtain all the dependent variables (Tu et al., 1991).

3. RESULTS

For a validation of the hydrodynamics model used for this study, the experiment of a turbulent hydraulic jet performed by Wu and Rajaratnam (1995) is chosen. The details about the experimental arrangement and flow conditions can be found in their paper and are not repeated here. A comparison of the predicted and measured jet velocity profiles is shown in Figure 3. The degree of agreement between the prediction and measurement is generally satisfactory.

The flow conditions for performing numerical experiments in this study are: the current velocity is u=0.0 and 0.2 m/s; the discharge velocity is v=0.8, 1.8, 2.1, 2.5 m/s for the physical model and v=4.0, 7.5, 9.0, 11.0, 13.0 m/s for the prototype, respectively. The Froude number at the outfall is defined by $F = v / \sqrt{gH}$, where g is the gravitational acceleration and H is the depth of water.

Figure 4 shows the mean velocity vector plots near the outfalls for both the physical model and prototype (the vectors are not scaled in order to visualise the main recirculation zone behind the discharge port). As mentioned before, the size of the main recirculation zone is characterised by its length L and lateral extent h (see Figure 1). Figures 5 and 6 show the variation of the size of the main recirculation zone with the Froude number. It is found that when the current velocity is equal to zero or very small, the size of the recirculation zone is independent of the discharge velocity. While the ocean flow has a current velocity 0.2 m/s, the recirculation zone behind the discharge port is rapidly expanding with the increase of the discharge velocity. It is also interesting to notice that in the case of the current velocity u=0.2 m/s the lateral extent of the recirculation zone in the prototype is larger than that in the physical model, which is entirely different from the situation in zero current velocity. The maximum discrepancy between the physical model and the prototype by measuring the mean characteristic size of the recirculation zone is about 20% in the current velocity u=0.0 m/s and less than 7% in u=0.2 m/s.

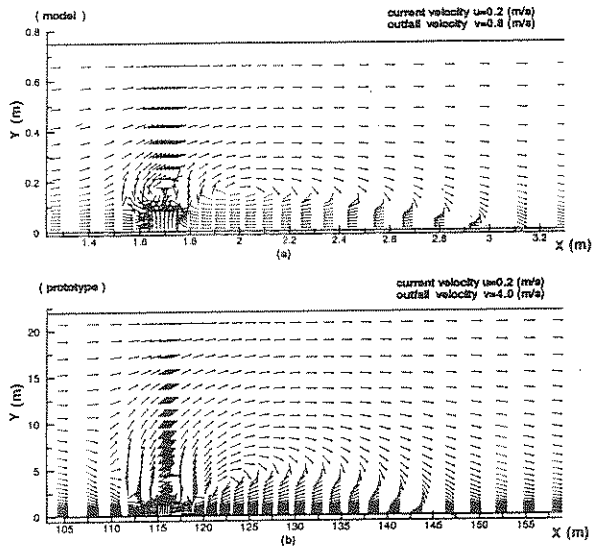

Figure 4 Mean velocity vector plots near the outfalls
(a) Physical model; (b) Prototype

The spatial distributions of the turbulent kinetic energy, k and its dissipation rate, ε, calculated from the two computational models with the different discharge velocities are shown in Figures 7-10. A main finding from this figures is that the distribution patten of both k and ε around the discharge port is significantly different between the phsical model and the prototype at both the samll (Figures 7 and 8) and large discharge velocities (Figures 9 and 10).

Comparison of the normalised turbulent kinetic energy, $k^*=k/(v^2)$ where v is the discharge velocity, and the normalised turbulent energy dissipation rate, $\varepsilon^*=\varepsilon/(v^3/H)$, between the physical model and the prototype are given in Figures 11 and 12, respectively. A normalised distance X^* is measured from the centre of the discharge port with the normalisation by the depth of water, H. The data in Figures 11 and 12 are taken along the distance of H/3 from the bottom of computational domain. The flow condition is the current velocity u=0.2 m/s; the discharge velocity v=0.8 m/s in the physical model and v=4.0 m/s in prototype, respectively.

It can be seen from Figure 11 that the higher turbulent kinetic energy in the mixing flow close to the discharge port in the prototype is observed than in the physical model. In the case of the prototype, the turbulent kinetic energy decays very rapidly within a short distance from the discharge port and then the mixing flow maintains at a lower turbulence level. In the case of the physical model, however, the turbulent kinetic energy does not decay as much as in the prototype and is overestimated to be twice higher than that in the prototype. A similar trend is also found for the turbulent energy dissipation rate as can be seen from Figure 12.

4. CONCLUDING REMARKS

Complex mixing flows near ocean outfalls in a physical model and in a prototype have been computationally investigated in detail, including the effects of discharge velocities and ambient currents. Mean momentum and mass conservation equations are solved for hydraulic flow using a finite volume scheme with a recently developed RNG-based k-ε turbulence model. Before the detailed numerical experiments are carried out, the theoretical hydraulic model used for the investigation is validated against the experimental data. The numerical results obtained from two computational models representing the physical model and the prototype are compared. It is found that the computed sizes of recirculation zone behind the discharge port for characterising the mean behaviour of the mixing flow show the reasonable agreement between the physical model and the prototype. However, the numerical results of turbulent kinetic energy and its dissipation rate show the significant difference in both the spatial distribution pattern and magnitudes which can be overestimated as twice high in the physical model as that in the prototype.

ACKNOWLEDGEMENT: This work is supported by ANSTO's Research and Development (R&D) project under the grant RED-1 with Dr Peter Airey being the Project Manager.

REFERENCE

Couriel, E.D., and Wilkinson, D.L., Near Field Physical Modelling, *Interim Report93/01/06, Australian Water and Coastal Studies Pty Ltd*, August, 1993.

Falconer, R.A., 1993, Flow and Water Quality Modelling in Coastal and Inland Water, *Journal of Hydraulic Research*, Vol.30, No.4, pp. 437-453, 1992.

Fletcher, C.A.J., *Computational Techniques for Fluid Dynamics*, Vol 2: Specific Techniques for Different Flow Categories, 2nd Edition, Springer, Heidelberg, 1991.

Orszag, A. and Yakhot, V., Renormalization Group Modeling and Turbulence Simulations, in *Near-Wall Turbulent Flows*, (Eds., R.M.C. So, C.G. Speziale and B.E. Launder) Elsevier Science Publishers B.V., pp 1031-1046, 1993.

Proni, J.R., Huang, H, and Dammann, W.P., Initial Dilution of Southeast Florida Ocean Outfalls, *Journal of Hydraulic Engineering*, Vol.120, No.12, pp. 1409-1425, 1994.

Rhie, C.M. and Chow, W.L., Numerical Study of the Turbulent Flow Past an Airfoil with Trailing Edge Separation, *AIAA Journal*, Vol.21, pp.1525, 1983.

Roid, W., *Turbulence Models and Their Application in Hydraulics*, International Association for Hydraulic Research, Delft, The Netherlands, 1980.

Tu, J. Y. and Fuchs, L., Calculation of Flows Using Three-Dimensional Overlapping Grids and Multigrid Methods, *Int. J. Numer. Methods Eng.* Vol. 38, pp. 259-282 1995.

Tu, J. Y., Fuchs, L. and Bai, X.S, Finite Volume and Multi Grid Methods on 3-D Zonal Overlapping Grids, *Multigrid Methods*, GMD-Studien, Nr-189, pp.337-348, 1991.

Van Doormaal, J.P. and Raithby, G.D., Enhancements for the SIMPLE Method for Predicting incompressible Fluid Flow, *Num. Heat Transfer*, Vol. 7, pp.147-163, 1984.

Wu, S., and Rajaratnam, N., Free Jumps, Submerged Jumps and Wall Jets, *Journal of Hydraulic Research*, Vol.33, No.2, pp. 197-212, 1995.

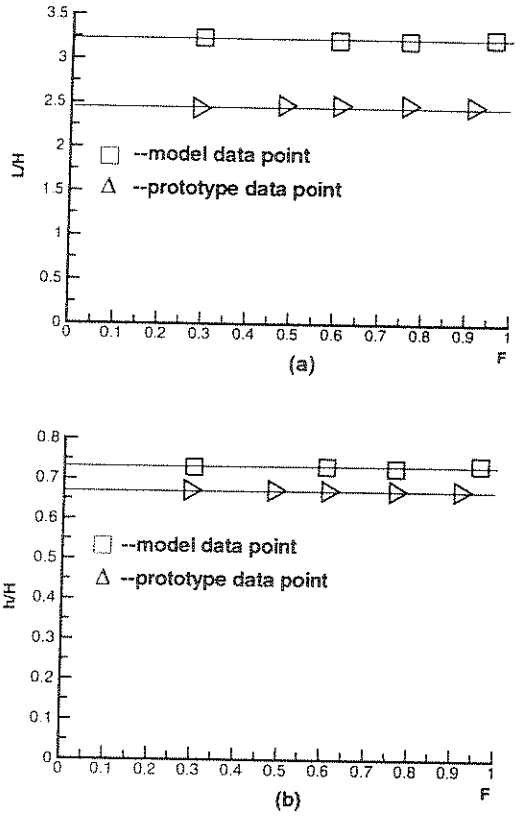

Figure 5 Variation of recirculation zone size with Froude number (u=0.0 m/s)

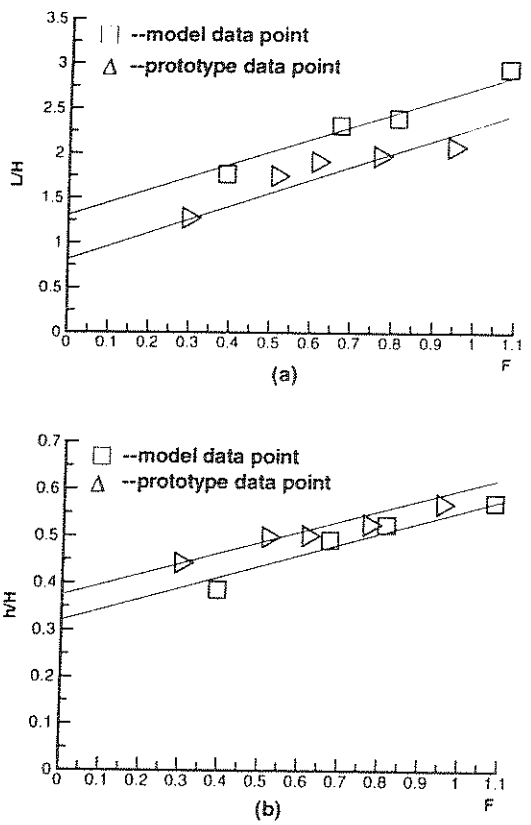

Figure 6 Variation of recirculation zone size with Froude number (u=0.2 m/s)

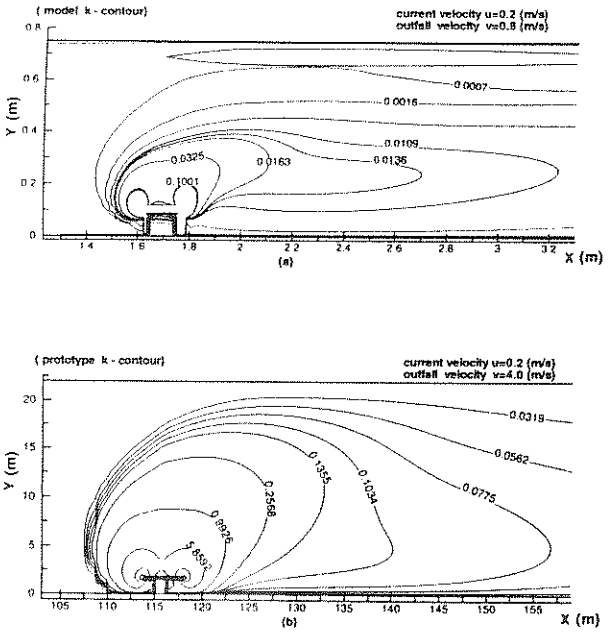

Figure 7 Calculated turbulent kinetic energy (a) Physical model; (b) Prototype

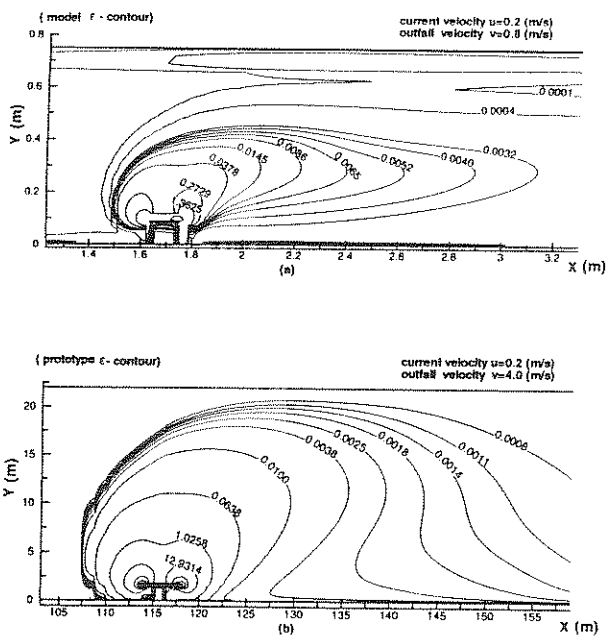

Figure 8 Calculated turbulent dissipation rate (a) Physical model; (b) Prototype

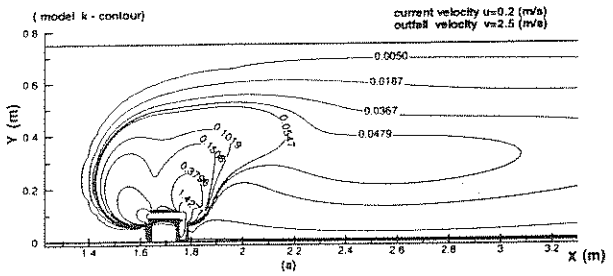

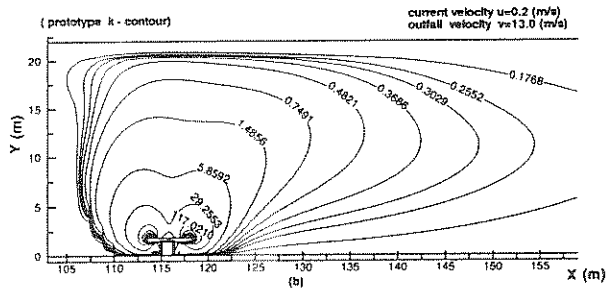

Figure 9 Calculated turbulent kinetic energy
(a) Physical model; (b) Prototype

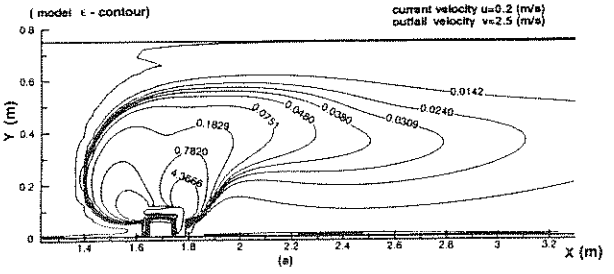

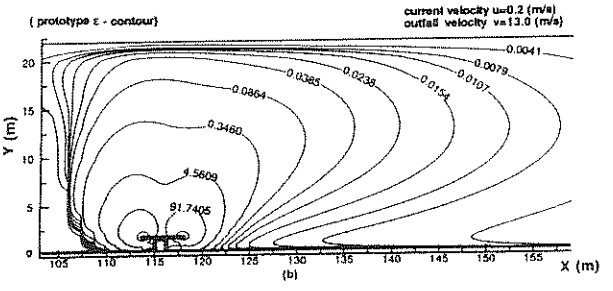

Figure 10 Calculated turbulent dissipation rate
(a) Physical model; (b) Prototype

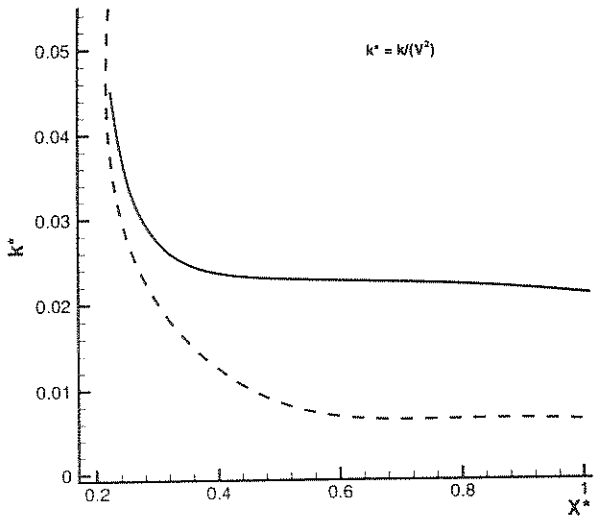

Figure 11 Normalised turbulent kinetic energy
—Physical model; - - - Prototype

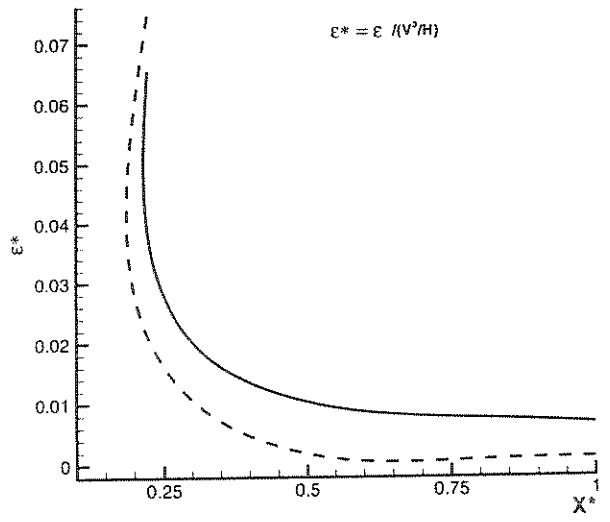

Figure 12 Normalised turbulent dissipation rate
—Physical model; - - - Prototype